Synthesis and Evaluation of Naphthalene Derivatives as Potent STAT3 Inhibitors and Agents Against Triple-Negative Breast Cancer Growth and Metastasis

Zhengyan Yang
Henan University
Hongyun Xu
Henan International Joint Lab for Anti-cancer Drug Design Based on Biological Target and Drug Discovery
Yupo Yang
Henan International Joint Lab for Anti-cancer Drug Design Based on Biological Target and Drug Discovery
Chaoqun Duan
Henan International Joint Lab for Anti-cancer Drug Design Based on Biological Target and Drug Discovery
Pai Zhang
Henan University
Yuan Zhou
Henan University
Xin Wang
Henan University
Pan Li
Henan University of Technology School of Chemistry and Chemical Engineering
Yang Wang
Huaihe Hospital of Henan University
Kai Fu
Nebraska Medicine-Nebraska Medical Center: Nebraska Medicine
Yonghong Shen
Henan University
Marvin Xuejun Xu (xumarvinxuejun@outlook.com)
Henan International Joint Lab for Anti-cancer Drug Design Based on Biological Target and Drug Discovery https://orcid.org/0000-0003-0413-7920

Research Article

Keywords: TNBC, STAT3, SMY002, Cyclin D1, MMP9

Posted Date: January 19th, 2022

DOI: https://doi.org/10.21203/rs.3.rs-1238979/v1

Abstract

Purpose Signal transducer and activator of transcription 3 (STAT3) has been reported to be hyper-activated in triple-negative breast cancers (TNBCs) and predicts poor outcomes. However, no drugs targeting STAT3 have been marketed. To develop STAT3 inhibitors for the treatment of TNBC, we synthesized and evaluated a new series of naphthalene derivatives.

Methods A new series of compounds with the scaffold of Selective Estrogen Receptor Modulator (SERM) and an amino group were designed and screened on the basis of the structure–activity relationship by MTT assay. The binding activity of SMY002 to STAT3 was predicted and validated by docking and SPR. The STAT3 signaling target and anti-cancer effect of SMY002 were evaluated by 3 three TNBC cell lines and the mice transplanted tumor model.

Results Among the compounds, SMY002 (2a) displayed the most potent activity, which could directly interact with STAT3 SH2-domain, and strongly inhibit phosphorylation, dimerization, nuclear distribution, transcriptional activity, and target genes expression of STAT3. Furthermore, SMY002 markedly suppressed migration, invasion, survival, growth, and metastasis of TNBC cells in vitro and in vivo via down-regulating the expression of Cyclin D1 and MMP9.

Conclusion The new compound SMY002 holds the potential of being developed into STAT3 inhibitory tools and TNBC treatment agents.

Introduction

Breast cancer has become the highest cancer incidence rate and is the leading cause of cancer-related mortality worldwide [1]. About 10-15% of BC patients are triple-negative breast cancers (TNBCs) [2]. Due to the lack of expression of estrogen receptor (ER), progesterone receptor (PR), and human epidermal growth factor receptor 2 (HER2), TNBC patients are insensitive to endocrine therapy and HER2-targeted drugs [3]. TNBC has substantial heterogeneity and invasiveness, is resistant to conventional chemotherapy, and is easy to relapse or metastasis in the early stage. The poor outcome highlights the necessity to exploit more efficacious agents for TNBC therapy.

Signal transducer and activator of transcription 3 (STAT3) is a crucial regulator of the glycoprotein 130 KD (GP130)/Janus kinases (JAKs)/STAT3 signaling pathway. It is primarily mediating signal transmission between the cytoplasm and nucleus [4]. When GP130, a media of STAT3 signal pathway) were binding with their ligands, their subunits were close up to form dimers, leading to the phosphorylation of Janus kinase 2 (JAK2), which in turn catalyzes the phosphorylation of tyrosine 705 (Tyr705) on SRC homology domain 2 (SH2) of STAT3[5–8]. STAT3 directly regulates various target genes expression, such as CCND1, BCL-XL, SURVIVIN, matrix metalloproteases (MMPs), and programmed cell death 1 ligand 1(PD-L1) [9–15]. These genes are associated with cancer proliferation, survival, angiogenesis, metastasis, and immune evasion. Extensive studies certified that STAT3 is overexpressed

or constitutively activated in most human malignant cancers, including TNBCs, and positively related to tumor progression [16–18].

Accumulated evidence proved that selective estrogen receptor modulators (SERMs) such as Badoxifene and Raloxifene exhibit anti-cancer effects by inhibiting IL-6/GP130/STAT3 signaling [19–21]. Here, we synthesized a new series of naphthylamine derivatives with the structure of 4-nitronaphthol and SERM as scaffolds. Among them, SMY002 can effectively inhibit the phosphorylation and transcriptional activity of STAT3 by interaction with the SH2 domain. Moreover, SMY002 suppressed the viability, survival, mobility, and dissemination of TNBC cells. Therefore, SMY002 holds the potential to be developed as STAT3 inhibitory tools or anti-TNBC treatment agents.

Materials And Methods

Chemical Synthesis

All reagents were purchased from commercial sources and used without further purification. NMR spectra were generated on a Bruker 500 MHz instrument. High-resolution mass spectra were gathered on a Bruker Micro-TOF-Q II LCMS instrument operating in electrospray ionization (ESI). High-pressure liquid chromatography (HPLC, Agilent Technologies 1200 Series) was conducted on an Eclipse XDB C18 column (5 μm, 4.6 mm × 150 mm) for purity Determination. All compounds are >95% pure by HPLC analysis.

Synthesis of methyl 4-(2-(piperidin-1-yl) epoxy) benzoate (2). The DIAD (17.3 g, 85.4 mmol) was purchased and added dropwise to a solution of methyl- 4-hydroxybenzoate (10 g, 65.7 mmol), 2-(piperidin-1-yl) ethan-1-ol (10.2 g, 78.9 mmol) and PPh3 (22.4 g, 85.4 mmol) in dry THF (200 ml) at 0°C under nitrogen. The reaction mixture was allowed to warm to room temperature and stirred for 12 h. After completion, the reaction mixture was concentrated by drying under reduced pressure. The residue was immersed in 1 N HCl aqueous solution (200 ml) and extracted with ethyl acetate 3 times (150 ml×3). The aqueous phase was adjusted to pH = 8 with solid sodium bicarbonate and extracted with ethyl acetate 3 times (150 ml×3), after which the combined organic layers were dried over anhydrous sulfate sodium and concentrated to give ethyl 4-(2-(piperidin-1-yl) epoxy) benzoate (2) as a white solid (10 g, 57.8% yield). 1H NMR (CDCl3, 300 MHz) δ: 8.0 (d, J = 9.0 Hz, 2H), 6.93 (d, J = 9.0 Hz, 2H), 4.17 (t, J = 6.0 Hz, 2H), 3.90 (s, 3H), 2.82 (t, J = 6.0 Hz, 2H), 2.58-2.55 (m, 4H), 1.66-1.61 (m, 4H), 1.50 (t, J = 3.0 Hz, 2H).

(4-(2-(piperidin-1-yl) ethyl) phenyl) methanol (3). LiAlH4 (1.44 g, 40 mmol) was slowly added to a solution of methyl-4-(2-(piperidin-1-yl) epoxy) benzoate (10 g, 40 mmol) in dry THF (200 ml) at 0°C. The mixture was stirred at 0°C for 30 min. After completion, 15% NaOH (1.5 ml) and water (1.5 ml) were added. The resulting mixture was filtered through a pad of Celite and rinsed with ethyl acetate. The filtrate was dried over a hydrous sulfate sodium and concentrated to give (4-(2-(piperidin-1-yl) ethyl) phenyl) methanol (3) as a white solid (8 g, 90% yield). 1H NMR (CDCl3, 300 MHz) δ: 7.30 (d, J = 6.0 Hz, 2H), 6.92 (d, J = 6.0 Hz, 2H), 4.64 (s, 2H), 4.17 (t, J = 6.0 Hz, 2H), 2.98 (t, J = 6.0 Hz, 2H), 2.74 (m, 4H), 1.89-1.86 (m, 6H).

1-(2-(4-(((4-nitronaphthalen-1-yl) foxy) methyl) phenol)-ethyl) piperidine (4). NaH (60%, 1.46 g, 36.6 mmol) was added to a solution of (4-(2-(piperidin-1-yl) ethyl) phe-yl) methanol (7.39 g, 31.4 mmol) in dry THF (100 ml) at 0°C under nitrogen, and the mixture was stirred at 0°C for 30 min. Then,1-fluoro-4-nitronaphthalene (5 g, 26.2 mmol) was added and stirred at room temperature for 12 h. After completion, the reaction mixture was poured into sat. NH4Cl (100 ml) and extracted with ethyl acetate 3 times (100 ml × 3). Combined organic layers were dried over anhydrous sulfate sodium and concentrated to give a residue. The residue was purified by silica gel column (elution with DCM/MeOH = 100/1 ~ 50/1) to give 1-(2-(4-LRB-4-nitronaphthalen-1yl) foxy) methyl) phenol) ethyl) piperidine (4) as a brown solid (7 g, 65.6% yield). 1H NMR (CDCl3, 400 MHz) δ: 8.81 (d, J = 8.0 Hz, 2H), 8.45-8.41 (m, 2H), 7.77-7.75 (m, 1H), 7.63-7.60 (m, 1H),7.47 (d, J = 8.0 Hz, 2H), 7.0 (d, J = 8.0 Hz, 2H), 6.93-6.90 (m, 1H), 5.32 (s, 2H), 1.89-1.86 (m, 6H), 4.37 (t, J = 6.0 Hz, 2H), 3.55-3.30 (m, 4H), 2.97 (t, J = 6.0 Hz, 2H), 1.79-1.67 (m, 4H), 1.65 (m, 4H), 1.39-1.20 (m, 2H).

Synthesis of 4-((4-(2-(piperidin-1-yl) ethyl) benzyl) foxy)-naphthalen-1-amine hydrochloride (SMY002). Fe (3.43 g, 61.5 mmol) was slowly added to a solution of 1-(2-(4–LRB-4-nitronaphthalen-1-yl) foxy) methyl) phenol) ethyl) piperidine (5 g, 12.3 mmol) in EtOH (50 ml). HCl (1 M, 20 ml) was added at 50°C, and the mixture was stirred at 50°C for 2 h. Then, the mixture was concentrated to remove EtOH, diluted with water (80 ml), and then extracted with DCM/MeOH (10/1, 100 ml × 3). Combined organic layers were dried over a hydrous sulfate sodium and concentrated to give a residue. The residue was purified by silica gel column (elution with DCM/MeOH =100/1~30/1) to give 4–LRB-4-(2-(piperidi-1-yl) ethyl) benzyl) foxy) naphthalen-1-amine hydrochloride (SMY002) as a red solid (2.3 g, 49.6% yield). 1H NMR (CDCl3, 300 MHz) 8.20 (d, J = 9.0 Hz, 1H), 8.13 (d, J = 9.0 Hz, 2H), 7.63-7.52 (m, 2H), 7.34-7.21 (m, 3H), 6.92 (d, J = 9.0 Hz, 1H), 6.82 (d, J = 9.0 Hz, 1H), 4.50 (s, 2H), 4.37 (t, J = 6.0 Hz, 2H), 3.55-3.30 (m, 4H), 2.97 (t, J = 6.0 Hz, 2H), 1.79-1.67 (m, 4H), 1.65 (m, 4H), 1.39-1.20 (m, 2H).

Cell Lines and Reagents

MCF-7, 4T1, MDA-MB-468, and MDA-MB-231 cell lines were obtained from the American Type Culture Collection (ATCC). 4T1, MCF-7, and MDA-MB-231 were grown in Dulbecco's modified Eagle's medium (DMEM, HyClone) supplemented with 10% FBS (Biological Industries, Israel). MDA-MB-468 cells were cultured with Leibovitz's L-15 Medium (Solarbio, China) containing 10% FBS in an incubator without CO2. Recombinant human interleukin-6 (rhIL-6) was obtained from R&D Systems. DMSO, MTT, and other conventional reagents without additional instructions were obtained from Sigma-Aldrich (US).

Computational Docking

We obtained the crystal structure of STAT3-SH2 domain from the RCSB protein data bank (PDB code: 1BG1) and prepared its structure by removing substructures, repairing the sidechains, adding hydrogens and charges with Auto Dock Vina [26]. The DFT calculations were carried out using the Gaussian 16 program package [27]. The geometry optimization of minima was carried out at the B3LYP-D3 level of theory [28] with the 6-31G(d) basis set. The results were obtained based on SCORE and the protein-compound complex analysis.

Surface Plasmon Resonance (SPR) Assay

The procedure was as described previously [29]. Briefly, phosphorylated and non-phosphorylated biotinylated EGFR-derived dodecapeptides containing the STAT3 peptide binding motif surrounding Y1068 were immobilized to CM5 chips (GE Healthcare, Sweden) [30]. The running buffer was prepared with the Tris buffer (20 mM, pH 8.0), mercaptoethanol (2 mM), and DMSO (5%). SMY002 was diluted by running buffer to 1, 3, 10, 30, 100, 300, 1000 μM and pre-incubated with STAT3 (phospho Y705) peptide (500 nM, Abcam, ab179551) at 4°C for 2 h. STAT3 (phospho Y705) peptide's binding to EGFR-derived dodecapeptides was measured at a flow rate of 10 μL/min for 2 min. The IC50 values were analyzed by the Biacore T200 Evaluation Software Version 3.0.

Cell Proliferation Assay

Cells were cultured in 96-well plates with a density of 5×103 per well in triplicate. The next day, SMY002 was added at a concentration range from 0.01 to 100 μM for 48 h. DMSO was utilized as the solvent. Cells exposed to SMY002-free DMSO were used as controls. The data was measured by MTT assay, compared with that of control cells, and converted to a percentage. The inhibitory effect was analyzed by GraphPad Prism 6.0.

Luciferase Assay

Cells were co-transfected with the STAT3-Luc Reporter gene plasmid (YT455, Biolab Technology of Beijing, China) and pRL-TK vector (Promega, US) at a ratio of 1:200 (w/w) with Lipofectamine 2000 (Invitrogen, US). 48 h later, SMY002 were adding to corresponding wells for another 24 h. Cells were extracted and assayed with the Dual-Luciferase Reporter Assay System (E1910, Promega, US). The luminescence values were examined by a multifunctional microplate reader (Varioskan Flash, Thermo-Fisher, US). The STAT3-dependent promoter activity was determined by the ratio of firefly luminescence value/Renilla luminescence value.

Real-Time PCR

The primers used were as follows: GCTGCGAAGTGGAAACCATC and CCTCCTTCTGCACACATTTGAA for CCND1; TGCATTGTTCCCATAGAGTTCCA and CCTGAATGACCACCTAGAGCCTT for BCL-XL; TGTACCGCTATGGTTACACTCG and GGCAGGGACAGTTGCTTCT for MMP9; and CACGATGGAGGGGCCGGACTCATC and TAAAGACCTCTATGCCAACACAGT for β-actin. Real-time PCR was analyzed using SYBR Green PCR Master Mix as recommended by the manufacturer (Thermo- Fisher, US). The cycle threshold (CT) values of target genes were standardized by that of β-actin. All the data was analyzed with the relative quantitative method (2-ΔΔCt).

Immunoblotting, Immunofluorescence and Immuno-histochemistry

Antibodies against p-JAK2 (3776), p-STAT3 (9134), JAK2 (3230), STAT3 (9139), p-ERK1/2 (4695), p-AKT (4691), CyclinD1 (55506), BCL-XL (2764), β-Actin (3700), and GAPDH (5174) used for western blot,

immunofluorescence or immunohistochemistry were ordered from Cell Signaling Technology (CST, USA). Human MMP9 primary antibody (A2095) was ordered from ABclonal Technology (China). The Alexa Fluor 488-labeled rabbit secondary antibody for immunofluorescence was from Thermo (US). The secondary antibody for immunohistochemistry was obtained from a two-step immunohistochemistry detection kit (PV-9000, ZSGB-Bio, China).

Zymography Assay

The secretion levels of MMP9 were analyzed with an MMP Zymography Assay Kit (P1700, Applygen, China). The cell culture supernatant was collected by pipettes and centrifuged (12,000 rpm, 15 min, 4°C), and then diluted with 2× nonreducing PAGE loading buffer (1:1), and 20 μl samples were loaded and separated directly. An SDS-PAGE gel containing MMP9 substrate protein (substrate G) was prepared. The electrophoresis and stain of gels were performed according to the standard procedures. Gels were scanned on the GelDoc XR System (Bio-Rad, US).

Wound-Healing Assay

Cells were plated in a monolayer with more than 90% fusion. A pipette tip was utilized to draw straight and evenly scratches in each well. Cells were rinsed with PBS. The culture solution was replaced with DMEM containing low serum (0.5% FBS) for each well, and SMY002 was added. Wound healing was observed and photographed with an Olympus CKX41 microscope system.

Transwell Assay

For migratory ability assay, 2×105 cells suspended with 100 μl DMEM were added to the upper chambers (8 μm pore sizes, Corning, US) and supplemented with or without SMY002. For invasive ability assay, the upper chamber was coated with 100 μl Matrigel (1 mg/ml, BD, US) prior to seed cells. 800 μl of DMEM containing 20% FBS was added into the lower chambers. Cultured for 48 h, cells were fixed with methanol for 30 min and stained with 0.1% crystal violet for 30 min at room temperature. The inserts were immersed twice with PBS. The membranes were photographed using an Olympus CKX41 microscope system and counted by ImageJ software.

Cell Cycle and Apoptosis Assays

Cells were trypsinized and rinsed with PBS. 1×106 cells were fixed in cold 70% ethanol (diluted with sterile water) for 2 h at 4°C. The follow-up operations followed the instructions of the DNA content detection kit (Solarbio, China). The fluorescence of PI-stained cells was read by a flow cytometer (BD, US) at the wavelength 630 nm and analyzed with Cell Quest software. Apoptosis assays were performed using the Annexin V-FITC apoptosis detection kit (Solarbio, China) by flow cytometry.

Animal Studies

All animal experiments were conduc-ted following the regulations of the Laboratory Animal Welfare and Ethics Committee and approved by the local authorities. Five-week-old female BALB/c mice were obtained from Beijing Vital River Laboratory Animal Technology. 4T1 cell suspension (1×10^5

cells/mouse) was subcutaneously injected into the mice. All mice were randomly divided into two groups with 5 mice in each group. After seven days of implantation, the mice were administered with PBS or SMY002 (30 mg/kg in PBS as a solvent) by daily gavage. The body weight and tumor sizes of mice were detected every other day. Four weeks after implantation, all mice were euthanized with isoflurane. The transplanted tumors were dissected, weighed, imaged, and fixed in 10% neutral formalin.

Statistical Analysis

All data are presented as the mean ± s.d. Two groups were compared by Student's t-test. For multiple group comparisons, statistical analyses were performed by one-way or two-way ANOVA using Graph-Pad Prism 6.0 software was considered signify-cantly different.

Results

Structure design, screening, and synthesis of SMY002

According to our previously unpublished results, compounds with 4-nitronaphthol as the parent nucleus have moderate antitumor activity. To explore more potent TNBC inhibitors, the structure of 4-nitronaphthol and SERM were used as the reference scaffold (Fig. 1A). Amino group replacing hydroxyl designation was introducing more polar interaction and amide group substituted by ethoxy group aimed to reduce steric hindrance between the phosphorylation binding site of STAT3 SH2 domain and compounds. Compounds were grouped and ranked in decreasing pharmacophore similarity in MTT assays against MDA-MB-231 cells (Fig. 1B). The compounds in the second group showed potent inhibitory activity, while Group compounds had weaker activity. The compounds in Group showed the minor potency in inhibiting cell viability.

Since SMY006 in Group showed the most potent activity (Fig. 1B), it was chosen for further study. By preparing and screening various of its salt compounds, we found that SMY002 (a kind of hydrochloride of SMY006) (Fig. 1C) with improved solubility and stability, had the best anti-proliferative activity (Fig. 1D).

The optimized synthesis steps of SMY002 were shown in Scheme 1. Compound 2 was synthesized by prepared compound Methylparaben and 2-Piperidinoethanol in the presence of PPh3 and DIAD through a mitsunobu reaction. Compound 2 was reduced by LiAlH4 in THF under 0°C to give compound 3. Compound 4 was obtained by Compound 3 and 1-Fluoro-4-nitrona-phthalene in the presence of NaH in THF through a nuclephilic reaction. Finally, compound 4 was reduced by Fe in 1N. HCl and EtOH mixture solvent to give SMY002. The synthetic details and spectrographic data of the intermediates and compound SMY002 were shown in Supplementary materials S1-4.

SMY002 directly interacts and binds to STAT3 with a high affinity

In predicting whether SMY002 interferes with the STAT3 protein, we obtained the crystal structure of STAT3-SH2 domain from the RCSB protein data bank (PDB code: 1BG1) and prepared its structure with Auto Dock Vina [22]. The DFT calculations were carried out using the Gaussian 16 program package. The geometry optimization of minima was carried out at the B3LYP-D3 level of theory [23] with the 6-31G(d) basis set. According to the computational docking, SMY002 (cyan) docked in the phospho-Tyrosine-binding pocket of the STAT3-SH2 motif (light blue) (Fig. 2A) [24]. Nine residues of Lys591, Glu594, Arg609, Ser613, Ile634, Ser636, Val637, Glu638, and Pro639 were found close to SMY002 (Fig. 2B). The model also indicates that SMY002 interacts stably with the Arg609 and Arg636 residues via 2 hydrogen bonds (black dash lines) (Fig. 2C). The ether bond oxygen atom in the ligand forms one hydrogen bond with the amine hydrogen atom on the branch chain of Arg609 (Fig. 2C). Meanwhile, the oxygen atom of the ether bond in the ligand forms the other hydrogen bond with the hydroxyl hydrogen atom of the Ser636 branched-chain (Fig. 2C). Thus, SMY002 might interact directly and stably with the STAT3 protein. The Surface Plasmon Resonance (SPR) experiments was carried out as described previously [25, 26]. The results showed that, SMY002 could compete blocking EGFR pY1068-peptide, the ligand of STAT3, for binding to Stat3 with IC50 values of 2 μM (Fig. 2D, 2E). These data manifested that SMY002 has a high affinity to STAT3.

The inhibitory effects of SMY002 on STAT3 activation

Then, the effects of SMY002 on the transcriptional regulatory function of STAT3 was detected. Fig. 3A shows that SMY002 treatment decreased the STAT3 Reporter gene activity in a dose-dependent manner. In addition, the downstream target genes of STAT3, such as CCND1 and BCL-XL, were also dramatically decreased at the mRNA expression level (Fig. 3B), which confirms that SMY002 inhibits the transcriptional activity of STAT3.

We further evaluated whether SMY002 suppresses the phosphorylation of STAT3 (Tyr705), which is crucial for its activation. Fig. 3C shows that the phosphorylation of Tyr705 on STAT3 was sharply elevated after stimulation with rhIL-6 (50 ng/ml) for 0.5 h in MCF-7 cells. The p-STAT3 (Tyr705) expression induced by rhIL-6 was abolished by SMY002 at 5 μM and completely inhibited at 10 μM. Similarly, SMY002 treatment suppressed STAT3 activation in a dose-dependent manner (Fig. 3D, 3E). Cyclin D1 expression was gradually down in corresponding with the change of p-STAT3. BCL-XL expression was also slightly decreased following SMY002 treatment. However, SMY002 did not impair the p-JAK2, p-ERK1/2, or p-AKT expression. These results displayed that SMY002 can specifically suppress STAT3 activation, not by inhibiting its upstream kinase JAK2 or other off-target effects but by directly interfering with STAT3 phosphorylation.

The dimerization and subcellular localization of p-STAT3 (Tyr705) is crucial for STAT3 binding to specific DNA elements. After SMY002 treatment, the inactive monomers of STAT3 were increased in a dose-dependent manner, which implies STAT3 dimerization were impeded (Fig. 3F). The nucleoprotein separation experiments show that SMY002 considerably diminished the expression of p-STAT3 (Tyr705) in both cytoplasm and nucleus (Fig. 3G). The same phenomenon was observed in MDA-MB-468 cells

(Fig. 3H). To further support this finding, the indirect immunofluorescence experiments were performed. As Fig. 3I shows that the nuclear localization of p-STAT3 (Tyr705) in MDA-MB-231 cells without SMY002 treatment was robust regardless of IL-6 stimulation. SMY002 treatment markedly reduced the nuclear staining of p-STAT3 (Tyr705). Therefore, SMY002 can impede the activation, dimerization, and nuclear localization of STAT3 by preventing the phosphorylation of Tyr705.

SMY002 inhibits the survival and cell cycle progression of TNBC

We next assessed the effect of SMY002 on survival and cycle progression of TNBC. The apoptosis ratio of MDA-MB-468 cells were increased from 1.75–17.54% and 54.47%, respectively, after treatment with SMY002 10 or 20 μM, (Fig. 4A,4B). Similar data were obtained in MDA-MB-231 cells (Fig. 4C). In addition, SMY002 induced significant G1 phase arrest and visibly shortened S phase in TNBC cells (Fig. 4D-4F). These results reveal that SMY002 substantially induces cell apoptosis and prolongs the cell cycle.

We next assessed the effect of SMY002 on survival and cycle progression of TNBC. The apoptosis ratio of MDA-MB-468 cells were increased from 1.75–17.54%, and 54.47%, respectively, after treatment with SMY002 10 or 20 μM, (Fig. 4A,4B). Similar data were obtained in MDA-MB-231 cells (Fig. 4C). In addition, SMY002 induced significant G1 phase arrest and visibly shortened S phase in TNBC cells (Fig. 4D-4F). These results reveal that SMY002 substantially induces cell apoptosis and prolongs the cell cycle.

SMY002 attenuates the motility of TNBC in vitro

One of the critical malignant phenotypes of TNBC cells is their potential for metastasis. To investigate whether SMY002 suppresses STAT3-promoted tumor cell migration, we evaluated the effect of SMY002 on TNBC cells migration by scratch assays. In comparison with the control, SMY002 treated cells showed significantly lower migration activities, as evidenced by the delay of wound closure were observed at different time points (Fig. 5A-5D). We utilized another approach, transit cell culture, to assess the cell migration and invasion abilities. Fig. 5E-5H results reveal that the control treatment cells displayed a remarkable capacity to pass through the membrane or invade through a reconstituted basement membrane (Matrigel) of a branchial chamber.

To explore why SMY002 inhibits cell migration and invasion, we detected the mRNA expression levels of a panel of genes by real-time Q-PCR. The data revealed that SMY002 treatment reduced the IL-10, COX2 (cytochrome oxidase subunit II), and MMP9, et al. expression (Fig. 5I, 5J), which were STAT3 target genes [27–29]. Then, we further detected the protein expression levels of MMP9 after treatment with SMY002 for 48 h in TNBC cells. Western blot results displayed that SMY002 repressed MMP9 expression in a dose-dependent manner (Fig. 5K, 5L). We performed a zymography assay to disclose the effect of SMY002 on MMP9 secretion. As shown in Fig. 5M, 5N, the transparent protein bands on the blue background of the stained gels, which indicate the location of MMP9, were weaker with increasing treatment with SMY002, demonstrating that SMY002 reduced the secretion of MMP9. Together, the above findings suggest that

SMY002 effectively suppressed the survival, cell cycle progression, mobility, and invasion of TNBC cells in vitro.

SMY002 reduced growth and metastasis of TNBC cells

We finally evaluated the therapeutic effect of SMY002 in 4T1 cells transplanted in mice. Compared with the vehicle (PBS) treatment group, SMY002 significantly reduced the volume and weight of tumors (Fig. 6A-6C). Xenografts in the SMY002 treatment group developed less lung metastasis than those in the vehicle group (white nodule in the metastatic loci decreased from 35 to 9.8) (Fig. 6D, 6E). Immunohistochemical staining results meant that p-STAT3 (Tyr705) and MMP9 expression in xenograft tumors treated with SMY002 was weaker than that of the vehicle group (Fig. 6F, 6G). These data are compatible with the in vitro results in Fig. 3-5 that SMY002 blocks the growth and invasion of TNBC cells via suppressing STAT3 activation. Compared with the vehicle group, the body weight of mice in SMY002 administration group was not significantly reduced (Fig. 6H). Additional adverse reactions, such as fever, bleeding or death, did not occur during the whole experiment, implying that SMY002 has few side effects in mice. Taken together, these data underlined that SMY002 potently suppressed the growth and dissemination of TNBC by inhibiting STAT3 activity.

Discussion

STAT3 possesses multiple functions in cancer development and has emerged as a critical therapeutic target in TNBCs. Accumulated studies elucidated that the excessive activation of STAT3 (Tyr705) plays a pivotal role in accelerate cell proliferation, survival, and the complex multistep process of cancer cell invasion by up-regulating the expression of down-stream targets at the transcriptional level. The SH2 domain contains specific recognition sites of phosphorylated tyrosine residues, which is of great significance for the phosphorylation, nucleation and dimerization of STAT3, so as to play the function of transcription factors.

In this study, a new series of naphthylamine compounds were designed and optimized as potent STAT3 inhibitors based on the hit compound of 4-nitronaphthol and SERMs. Among them, SMY002 showed the best antiproliferative activity. It inhibited the phosphorylation, nuclear translocation, dimerization, transcriptional activity, and target genes expression of STAT3 by interaction with the STAT3 SH2 domain. However, it did not affect the activity of JAK2, which is an essential upstream modulator of STAT3, or the phosphorylation of ERK1/2 and AKT, which are also recognized as critical signals for cancer cell survival. Thus, SMY002 has a selective and direct inhibitory effect on STAT3 activity. Moreover, SMY002 could impede the survival and mobility of TNBC cells. Preliminary in vivo experiments revealed that SMY002 remarkably reduced the growth and dissemination of transplanted TNBC cells in mice. Further studies on pharmacokinetics and toxicology will be carried out to ensure the application of SMY002 in TNBC therapy.

Taken together, these data indicated that SMY002 could repress the malignant biological behavior of TNBC cells by blocking the phosphorylation and activation of STAT3 (Tyr705). Further development of

these new naphthylamine compounds synthesized with 4-formyl-phenol as substrate may provide potential opportunities for the targeted therapy of TNBC in the future.

Abbreviations

STAT3, signal transducer and activator of transcription 3

TNBC, triple-negative breast cancer

SERM, selective estrogen receptor modulator

ER, estrogen receptor

PR, progesterone receptor

HER2, human epidermal growth factor receptor 2

GP130, glycoprotein 130 KD

JAKs, Janus kinases

SH2, SRC homology domain 2

MMPs, matrix-metalloproteases

PD-L1, programmed cell death 1 ligand 1

Tyr705, tyrosine 705

IC50, half maximal inhibitory concentration

DMSO, dimethyl sulfoxide

SPR, surface plasmon resonance

MTT, 3-(4,5-dimethylthiazol)-2,5-diphenyltetrazolium bromide

DAPI, 4,6-diamidino-2-phenylindole

COX2, cytochrome oxidase subunit II

Declarations

Acknowledgements

This work was supported by grants from High-End Foreign Experts Introduction Plan of Henan Science and Technology Department (No. G20190126005), Kaifeng Science and Technology Development Plan Project (No. 21SSF003), Youth Fund of National Natural Science Foundation of China (No. 81803575 and 31902287), Key Scientific Research Project of Colleges and Universities in Henan Province (No. 19A310006).

Declaration of Competing Interest

The authors have declared no conflict of interest.

References

1. Siegel MPH, Rebecca L, Kimberly D, Miller MPH, Hannah E, Fuchs BS (2021) Ahmedin Jemal DVM,PhD. Cancer Statistics, 2021. CA Cancer J Clin 71(1):7–33
2. Kumar P, Aggarwal R (2016) An overview of triple-negative breast cancer. Arch Gynecol Obstet 293(2):247–269
3. Jhan JR, Andrechek ER (2017) Triple-negative breast cancer and the potential for targeted therapy. Pharmacogenomics 18(17):1595–1609
4. Bromberg JF, Wrzeszczynska MH, Devgan G, Zhao Y, Pestell RG, Albanese C, Darnell JE Jr (1999) Stat3 as an oncogene. Cell 98(3):295–303
5. Darnell JJ, Kerr IM, Stark GR (1994) Jak-STAT pathways and transcriptional activation in response to IFNs and other extracellular signaling proteins. Science 264(5164):1415–1421
6. Katz M, Amit I, Yarden Y (2007) Regulation of MAPKs by growth factors and receptor tyrosine kinases. Biochim Biophys Acta 1773(8):1161–1176
7. Becker S, Groner B, Muller CW (1998) Three-dimensional structure of the Stat3 beta homodimer bound to DNA. Nature 394(6689):145–151
8. Klemm JD, Schreiber SL (1998) Crabtree. Dimerization as a regulatory mechanism in signal transduction. Annu Rev Immunol 16:569–592
9. Leslie Kenneth C, Lang G, Devgan J, Azare M, Berishaj W, Gerald YB, Kim K, Paz JE, Darnell C, Albanese T, Sakamaki R, Pestell J (2006) Bromberg. Cyclin D1 is transcriptionally regulated by and required for transformation by activated signal transducer and activator of transcription 3. Cancer Res, 66(5): 2544-2552
10. Grad JM, Zeng XR, Boise LH (2000) Regulation of BCL-XL: a little bit of this and a little bit of STAT. Curr Opin Oncol 12(6):543–549
11. Li W, Lee M-R, Kim T, Kim YW, Cho M-Y (2018) Activated STAT3 may participate in tumor progression through increasing CD133/survivin expression in early stage of colon cancer. Biochem Biophys Res Commun 497(1):354–361
12. Shi M, Liu D, Duan H, Han C, Wei B, Qian L, Chen C, Guo L, Hu M, Yu M, Song L, Shen B, Guo N (2010) Catecholamine up-regulates MMP-7 expression by activating AP-1 and STAT3 in gastric cancer. Mol

Cancer 9(12):269

13. Fukuda A, Wang SC, Folias AE, Liou A, Kim GE, Akira S, Boucher KM, Firpo MA, Mulvihill SJ, Hebrok M (2011) Stat3 and MMP7 contribute to pancreatic ductal adenocarcinoma initiation and progression. Cancer Cell, 19(4): 441-455
14. Shan Q, Li S, Cao Q, Yue C, Niu M, Chen X, Shi L, Li H, Gao S, Liang J, Yu R, Liu X (2020) Inhibition of chromosomal region maintenance 1 suppresses the migration and invasion of glioma cells via inactivation of the STAT3/MMP2 signaling pathway. Korean J Physiol Pharmacol 24(3):193–201
15. Sailan Zou Q, Tong B, Liu W, Huang Y, Tian (2020) Xianghui Fu. Targeting STAT3 in Cancer Immunotherapy. Mol Cancer 19(1):145
16. Jiang-Jiang Qin, Li Y, Zhang J, Zhang W-D (2019) STAT3 as a potential therapeutic target in triple negative breast cancer: a systematic review. J Exp Clin Cancer Res 38(1):195
17. Dongyao Wang X, Zheng B, Fu Z, Nian Y, Qian R, Sun Z, Tian, Haiming Wei (2019) Hepatectomy promotes recurrence of liver cancer by enhancing IL-11-STAT3 signaling. EBioMedicine 46:119–132
18. Christina Heichler K, Scheibe A, Schmied CI, Geppert B, Schmid S, Wirtz O-M, Thoma V, Kramer, Maximilian J, Waldner C, Buttner HF, Farin M, Pesic F, Knieling S, Merkel A, Gruneboom M, Gunzer R, Grutzmann S, Rose-John, Sergei B, Koralov G, Kollias M, Vieth A, Hartmann, Florian R, Greten, Markus F, Neurath (2020) STAT3 activation through IL-6/IL-11 in cancer-associated fibroblasts promotes colorectal tumour development and correlates with poor prognosis. Gut 69(7):1269–1282
19. Schott AF, Goldstein LJ, Cristofanilli M, Ruffiffiffini PA, McCanna S, Reuben JM, Perez RP, Kato G, Wicha MS (2017) Phase Ib Pilot Study to Evaluate Reparixin in Combination with Weekly Paclitaxel in Patients with HER-2-Negative Metastatic Breast Cancer. Clin Cancer Res 23:5358–5365
20. Tian J, Chen X, Fu S, Zhang R, Pan L, Cao Y, Wu X, Xiao H, Lin HJ, Lo HW, Zhang Y, Lin J (2019) Bazedoxifene is a novel IL-6/GP130 inhibitor for treating triple negative breast cancer. Breast Cancer Res Treat 175(3):553–566
21. Li H, Xiao H, Lin L, Jou D, Kumari V, Lin J, Li C (2014) Drug Design Targeting Protein-Protein Interactions (PPI) Using Multiple Ligand Simultaneous Docking (MLSD) and Drug Repositioning: Discovery of Raloxifene and Bazedoxifene as Novel Inhibitors of IL-6/GP130 Interface. J Med Chem 57(3):632–641
22. Trott Oleg, Olson Arthur J, AutoDock, Vina (2010) Improving the speed and accuracy of docking with a new scoring function, efficient optimization, and multithreading. J Comput Chem 31(2):455–461
23. Grimme S, Antony J, Ehrlich S, Krieg H (2010) A consistent and accurate ab initio parametrization of density functional dispersion correction (DFT-D) for the 94 elements H-Pu. Journal of Chemical Physics 132(15):154104–154124
24. Becker S, Groner B, Muller CW (1998) Three-dimensional structure of the Stat3beta homodimer bound to DNA. Nature 394(6689):145–151
25. Xuejun Xu MM, Kasembeli X, Jiang BJ, Tweardy DJ (2009) Tweardy. Chemical Probes that Competitively and Selectively Inhibit Stat3 Activation. PLoS ONE 4(3):e4783

26. Shao H, Xu X, Mastrangelo M-AA, Jing N, Cook RG, Legge GB, Tweardy DJ (2004) Structural Requirements for Signal Transducer and Activator of Transcription 3 Binding to Phosphotyrosine Ligands Containing the YXXQ Motif. J Biol Chem 279:18967–18973
27. Campana L, Lewis PJS, Pellicoro A, Aucott RL, Man J, O'Duibhir E, Mok SE, Gonzalez SF, Livingstone E, Greenhalgh SN, Hull KL, Kendall TJ, Vernimmen D, Henderson NC, Boulter L, Gregory CD, Feng Y, Anderton SM, Forbes SJ, Iredale JP (2018) The STAT3-IL-10-IL-6 Pathway Is a Novel Regulator of Macrophage Efferocytosis and Phenotypic Conversion in Sterile Liver Injury. J Immunol 200(3):1169–1187
28. Ren M, McGowan E, Li Y, Zhu X, Lu X, Zhu Z, Lin Y, He S (2019) Saikosaponin-d Suppresses COX2 Through p-STAT3/C/EBPbeta Signaling Pathway in Liver Cancer: A Novel Mechanism of Action. Front Pharmacol 10:623
29. Jia ZH, Jia Y, Guo FJ, Chen J, Zhang XW, Cui MH (2017) Phosphorylation of STAT3 at Tyr705 regulates MMP-9 production in epithelial ovarian cancer. PLoS ONE 12(8):e0183622

Scheme

Scheme 1 is available in supplementary section.

Figures

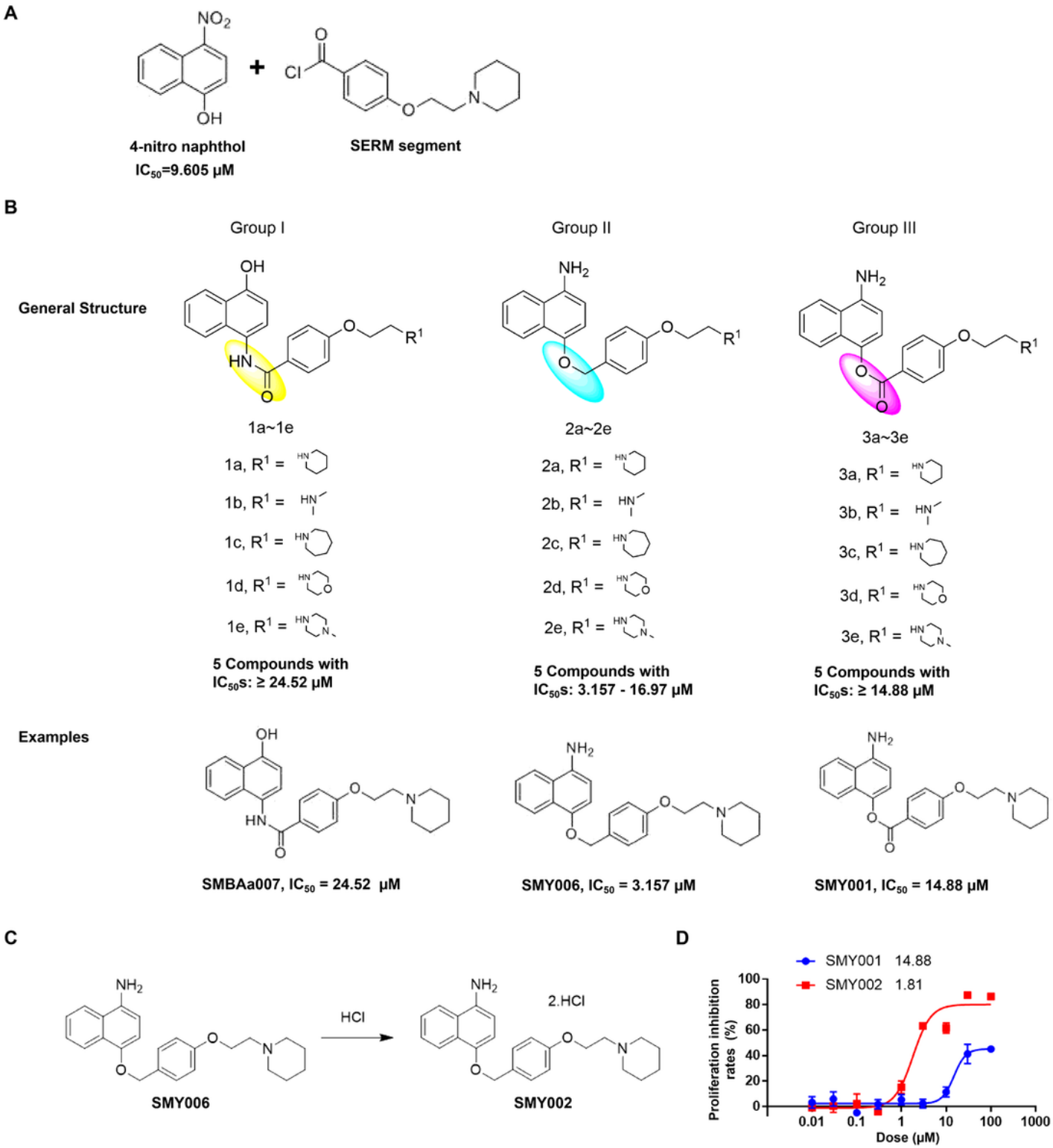

Figure 1

Structure design and synthesis of naphthalene derivatives. A, The initial hit compounds of 4-nitronaphthol and a segment of SERMs general structure. B, Structural characteristics and groupings of potential TNBC inhibitors. C, SMY002, a kind of hydrochloride of SMY006. D, Anti-proliferation activity of SMY002 and SMY001 against MDA-MB-231 cells was detected by MTT assay.

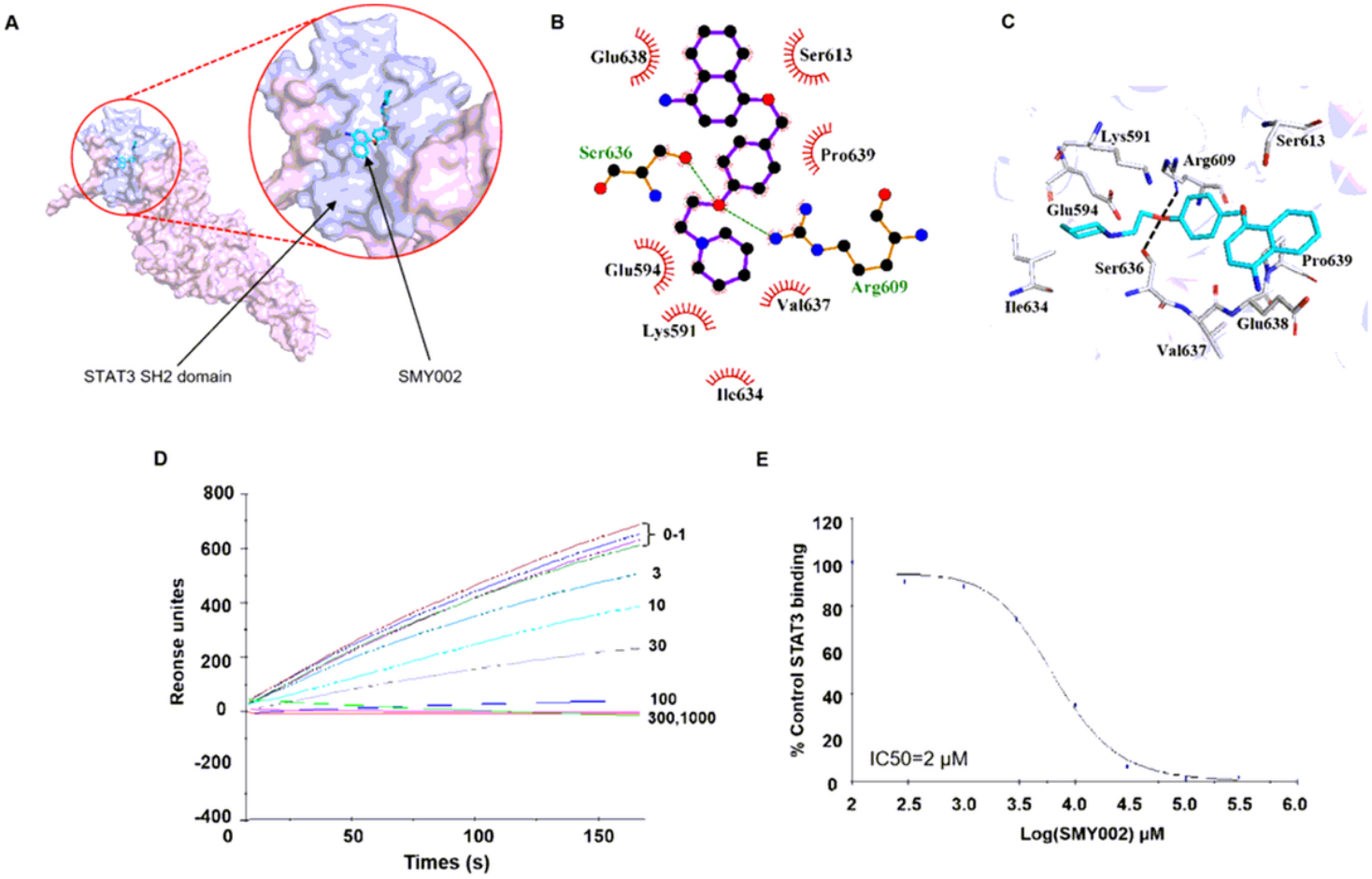

Figure 2

Docking and SPR assay of SMY002. A, Surface structure of STAT3 and ligand SMY002, the color in light blue is STAT3 SH2 domain. B, The schematic diagram of the interactions between STAT3 SH2 domain and SMY002. C, Residues R609 and S613 have hydrogen-bonding with SMY002, respectively. Interaction mode and affinity assay of SMY002 with STAT3 protein. D, Binding of recombinant STAT3 (500 nM) to Biacore sensor chip-coated with the phosphododecapeptide ligand (surrounding pY1068 of the EGFR) containing SMY002 (1 to 1000 μM) was measured by SPR. E, The competitive binding curve and IC50 value of SMY002 to STAT3 in the SPR assay.

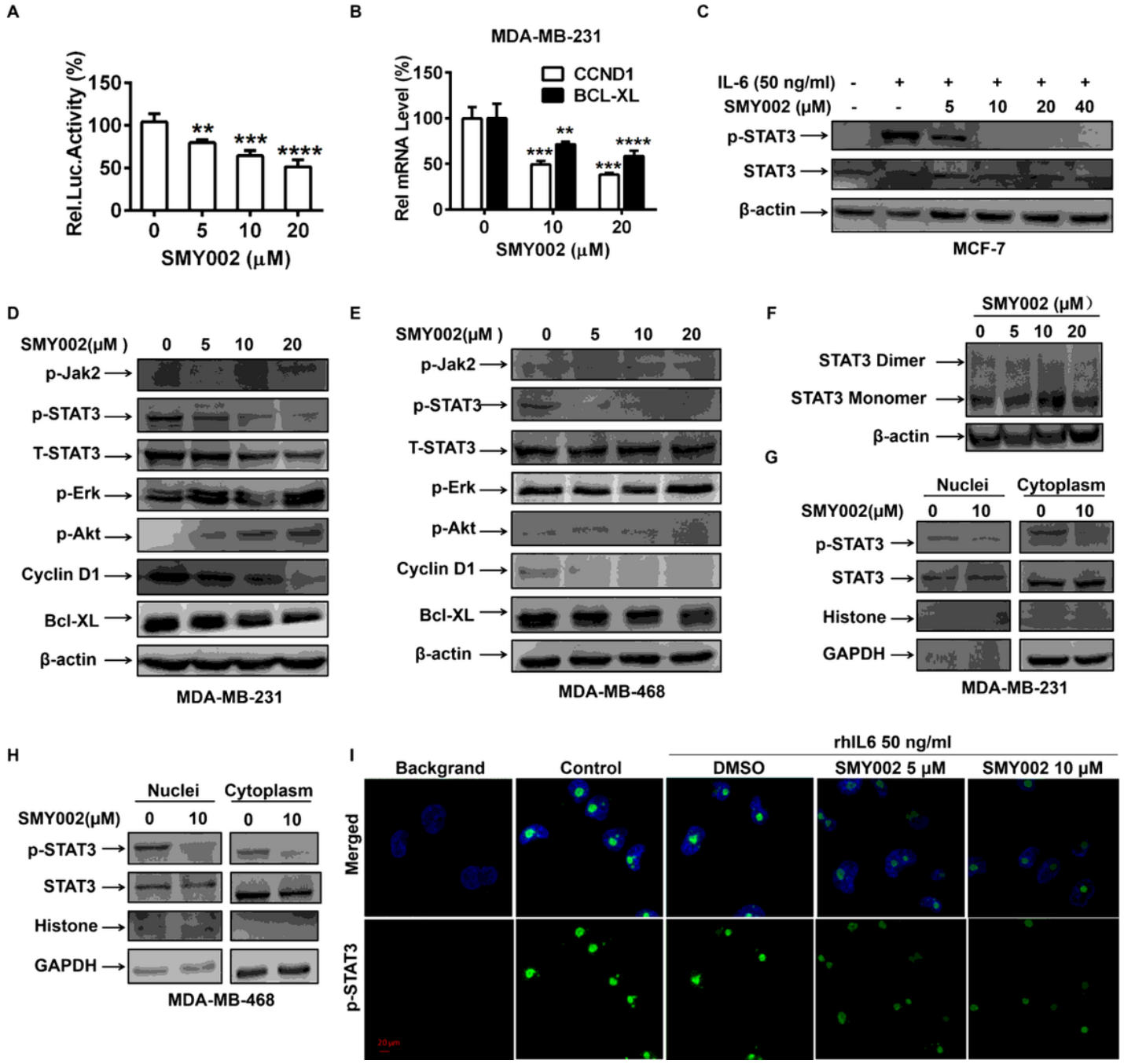

Figure 3

SMY002 inhibits the phosphorylation and activation of STAT3. A, Luciferase assay of MDA-MB-231 cells treated with SMY002 for 48 h. B, Effects of SMY002 on CCND1 and BCL-XL mRNA expression were exammed by real-time PCR. C, MCF-7 cells were supplemented with various doses of SMY002 and 50 ng/ml rhIL-6 for 0.5 h. STAT3, p-STAT3 (Tyr705), and β-actin expression were analyzed by Western blot. D, E, Cells were treated with different doses of SMY002 for 48 h. The protein expression levels of p-JAK2 (Y1007/1008), p-STAT3 (Tyr705), T-STAT3, p-ERK 1/2, p-Akt (Ser473), Cyclin D1, BCL-XL, and β-actin were assayed by Western blot. F, MDA-MB-231 cells were incubated with SMY002 in various concentrations for 48 h and then extracted. The cell lysis mixture was separated using a non-denaturing PAGE. STAT3 dimers and monomers were detected by Western blot with the STAT3 antibody. G, H, Cells were dealt with

or without SMY002 for 24 h, followed by nuclear and cytoplasmic fractionation. The expression of p-STAT3 (Tyr705), total STAT3, Histone 3, and GAPDH was analyzed by Western blot. I, Cells were incubated with SMY002 (0, 5 or 10 μM) and rhIL-6 (50 ng/ml) for 0.5 h. Then p-STAT3 was detected by immunofluorescence in Alexa Fluor 488 channel. DAPI was utilized to stain nuclei. Cells were not incubated with primary antibodies were used as background control. Bars, 20 μm. (***p<.01, ***p<.001, ****p<.0001).*

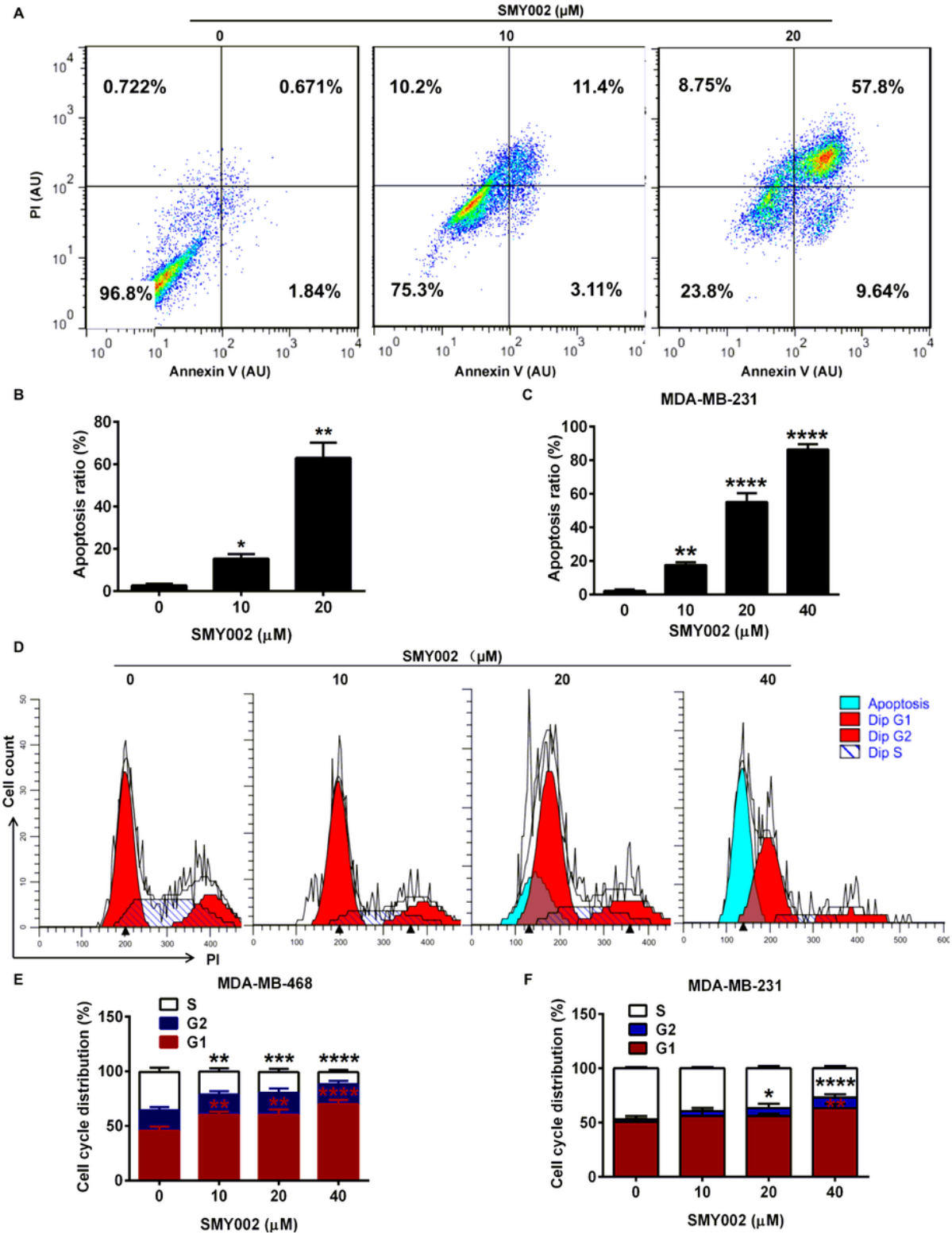

Figure 4

SMY002 induces cell apoptosis (A-C) and cycle blockage (D-E) in TNBC cells. (**p<.05, **p<.01, ***p<.001, ****p<.0001*).

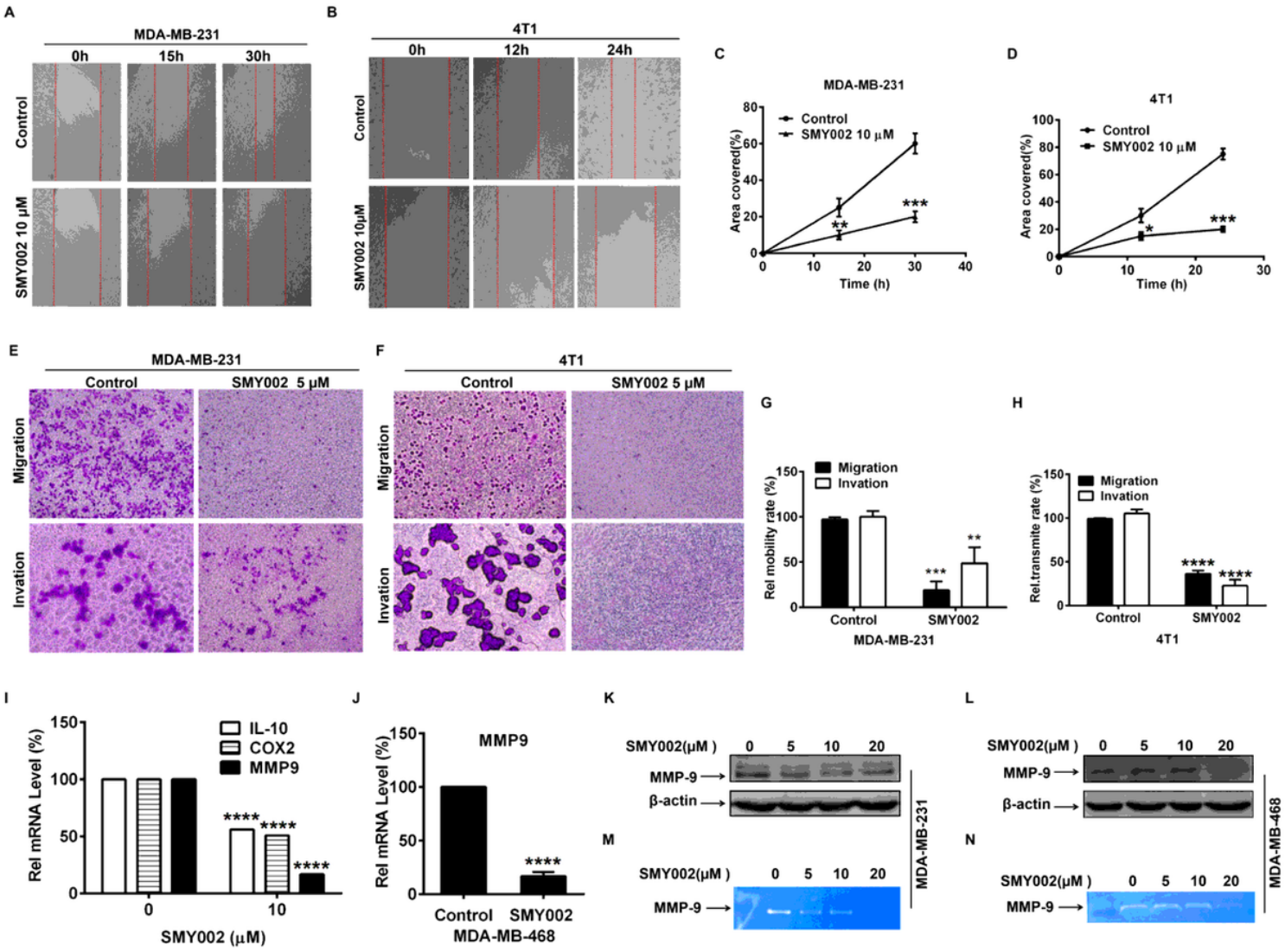

Figure 5

SMY002 attenuates the migration and invasion of TNBC cells in vitro. A, B, MDA-MB-231 and 4T1 cells were scratched and treated with or without SMY002 was imaged at indicated times. C, D, The healing area was calculated with Image J software. SMY002 inhibited cell migration and invasive activities were examined by the transit chamber assays. E-H, Cells that transited the filter membranes of chambers were photographed and counted by ImageJ software. I-L, TNBC cells were cultured with SMY002 for 48 h. Secreted MMP9 in the supernatant of cell culture was pipetted, centrifuged, concentrated, and then analyzed by zymography. MMP9 expression was analyzed by real-time PCR (I, J), Western blot (K, L), and zymography (M, N). (***p<.01, ***p< .001, ****p<.0001*)

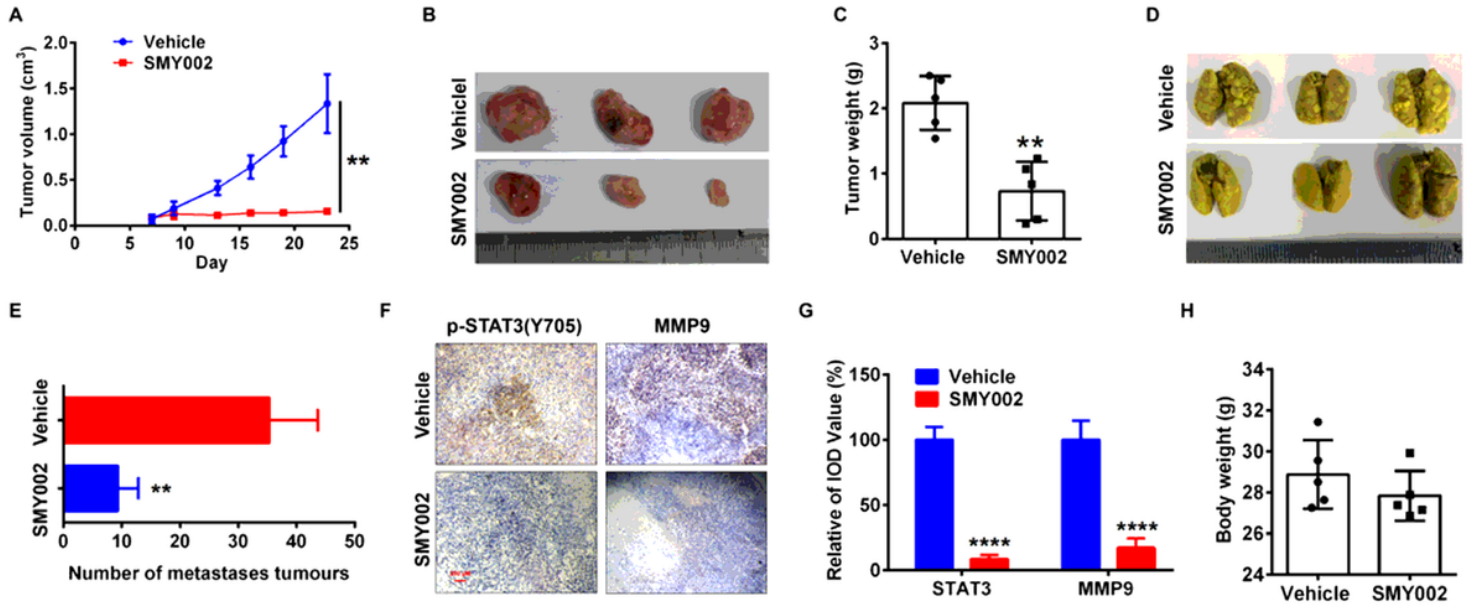

Figure 6

SMY002 prevents xenograft TNBC cells growth and dissemination in vivo. A, The volume of transplanted tumors with vehicle (PBS) or SMY002 administration. B, C, Gross anatomy (B) and wet weight (C) of primary tumors were photographed and recorded. D, E, Lungs of mice in the experimental group and the placebo group were dissected and fixed in the Bouin's solution. The white nodules that represented the tumor metastasis were imaged (D) and counted (E). F, G, Expression of p-STAT3 (Tyr705) and MMP9 in the xenograft tumors was assayed by IHC using specific antibodies (F) and quantified by Image-Pro Plus 6.0 (G), Bars, 200 μm. H, Body weight of mice before they were executed. (***p<.01, ****p<.0001*).

Supplementary Files

This is a list of supplementary files associated with this preprint. Click to download.

- Scheme1.tif